

Limitations of Debye-Waller lattice temperature extraction under electronic excitation

N. Medvedev^{1,2,*}, M. Kopecky¹, J. Chalupsky¹ L. Juha¹

1) *Institute of Physics, Czech Academy of Sciences, Na Slovance 1999/2, 182 00 Prague 8, Czechia*

2) *Institute of Plasma Physics, Czech Academy of Sciences, Za Slovankou 3, 182 00 Prague 8, Czechia*

Abstract

Ultrafast diffraction is the cutting-edge technique to extract the atomic temperature at femtosecond timescales, and further related quantities – in particular, electron-phonon coupling strength at elevated electronic temperatures. The present work demonstrates limitations of such an analysis, emphasizing the importance of careful evaluation of the evolution of the Debye temperature. It is shown that, due to the sensitivity of the Debye-Waller analysis to this parameter, neglecting its changes under electronic excitation may lead to significant deviations of the atomic temperature extracted from its true values.

Introduction

Ultrafast energy deposition drives matter into transient states outside of its equilibrium phase diagram [1–4]. Unique phases produced inspire both fundamental and applied interest. From the application point of view, some of the novel phases may be stabilized, creating unique material properties unachievable by other means [5–7]. The basic science interest lies in the kinetic pathways leading to the formation of the exotic states of matter.

The far-from-equilibrium kinetics of irradiated matter is still poorly understood [8,9]. General picture of the processes triggered by ultrafast irradiation is as follows: the laser photon absorption leads to excitation of the electronic ensemble at femtosecond timescales [10,11]. It drives the electronic distribution function to a nonequilibrium state, deviating strongly from the Fermi-Dirac function [12–14]. Electron-electron interaction then thermalizes the electronic ensemble at a temperature high above the atomic (phononic) one [11]. This process typically takes place at femtosecond timescales in metals, but may be prolonged in bandgap materials, requiring equilibration of the valence-band and conduction-band electrons [14,15].

This produces a transient two-temperature state, in which the hot electronic and the cold atomic ensembles have vastly different temperatures [11,16]. Simultaneously, the atomic (or phononic) system may also be out of equilibrium [17,18]. Furthermore, excitation of electrons may cause modification of the interatomic potential, which typically leads to a phonon hardening effect in metals, or nonthermal melting in non-metals [2,3,19,20].

The least known parameter is the electron-phonon coupling strength, defining the rate of energy exchange between the electronic and atomic subsystems in matter [8,9]. Without understanding the mechanism of such energy exchange, it is impossible to describe the

* Corresponding author: nikita.medvedev@fzu.cz; ORCID: 0000-0003-0491-1090

evolution of the system triggered by irradiation and production of the final observable material states.

Experimental probe of those processes is notoriously difficult. It requires ultrafast pumping of the system to induce nonequilibrium dynamics, and an ultrafast probe, measuring the transient states of matter [21,22]. The electron-ion (electron-phonon) coupling at high electronic temperatures is not a directly measurable quantity.

There are, currently, two approaches to extract it from experimental data: generally, one of them includes tracing the evolution of the electronic system and attempting to connect it with the energy sink into the atomic one. Such methods as XANES and electron spectroscopy were used, combined with the two-temperature model simulation to infer the corresponding coupling strength [23–25]. The drawback of such an approach is that the measured spectra are sensitive to the state of the electronic structure much more than to the electron-phonon coupling, and nonthermal effects and other modifications in the electronic structure may strongly influence the interpretation of the measurements [26].

The other approach is to probe the atomic state and extract the electron-phonon coupling from the evolution of the atomic (phononic) ensemble [26–28]. It is commonly assumed that the ultrafast probe of the atomic diffraction patterns enables extracting the transient atomic temperature, and therefore tracing its increase due to electron-phonon coupling [19,26,27,29].

Here, we demonstrate that the extraction of the atomic temperature from the diffraction patterns is not straightforward, and application of the Debye-Waller analysis may lead to incorrect estimates of the transient atomic temperatures.

Model

A state-of-the-art multiscale code, XTANT-3, is applied here to simulate the evolution of the diffraction reflections in various materials under irradiation [30]. The code combines various approaches to simultaneously trace the evolution of electronic and atomic systems. It includes the Monte Carlo simulation of photon absorption, electron impact ionization, and Auger decays of core-holes, if any are produced [31]. The Boltzmann collision integrals describe electron-electron relaxation and thermalization, as well as electron-ion coupling and energy exchange [14,32]. The transferrable tight binding method traces the evolution of the electronic structure (band structure) and the interatomic potential induced by the electronic excitation, including nonthermal melting or phonon hardening [14,31,33]. The molecular dynamics simulation propagates the atomic trajectories on the evolving potential energy surface, in response to the electronic excitation and electron-phonon coupling.

Having atomic coordinates in the simulation enables us to calculate the diffraction peaks' intensities for chosen Miller indices [34]:

$$I(\mathbf{q}) = \sum_{j=1}^{N_{at}} \sum_{k=1}^{N_{at}} f_j(\mathbf{q}) f_k(\mathbf{q}) \exp(-i\mathbf{q}(\mathbf{R}_j - \mathbf{R}_k)), \quad (1)$$

where $f_j(\mathbf{q})$ is the atomic form-factor of atom j among all the atoms in the supercell, N_{at} [35]; \mathbf{R}_j are the coordinates of the atoms j , and \mathbf{q} is the transferred momentum from the scattering X-ray photon.

Within the Debye-Waller (DW) approximation, Eq.(1) reduces to the following:

$$I(\mathbf{q}) = I_0(\mathbf{q}) \exp\left(-\frac{1}{3}q^2\langle u^2\rangle\right) = I_0(\mathbf{q}) \exp\left(-2q^2 \frac{3\hbar^2 T_a}{Mk_B\theta_D^2}\right) \quad (2)$$

Where I_0 is the initial (room-temperature) diffraction intensities; $\langle u^2\rangle = \frac{1}{N_{at}} \sum_{j=1}^{N_{at}} (\mathbf{R}_j - \mathbf{R}_j(t=0))^2$ is the mean square atomic displacement from its original positions; M is the atomic mass; k_B is the Boltzmann constant; \hbar is the Planck's constant; θ_D is the Debye temperature; and T_a is the atomic temperature.

Numerical details of the simulations are presented in the Supplementary Materials.

Results

We applied XTANT-3 to simulate the irradiation of copper with a pulse of $\lambda=400$ nm wavelength, $\tau=130$ fs full-width at half-maximum (FWHM) duration, $D=0.83$ eV/atom absorbed dose (corresponding to the experimental dose of 1.26 MJ/kg in Ref. [26]), and gold irradiated with the same pulse parameters and the dose $D=0.69$ eV/atom (0.36 MJ/kg in Ref. [27]). Figure 1 presents the results of diffraction peaks intensities simulated with XTANT-3 and those from the experimental measurements. They are in reasonable agreement for both materials up to the time of ~ 10 -12 ps.

The sudden drop of the simulated peaks after that time is an artifact of the finite-size effects in the simulation. Since the simulation boxes contained only 256 atoms, as soon as a single nucleation center of the liquid phase occurs, the entire box transitions into the liquid phase, and the diffraction peaks disappear. To replicate the smooth tails at longer times, it would require significantly larger simulation boxes (ideally, approaching the experimental material thickness of 30-50 nm), which is beyond the current capabilities of the model.

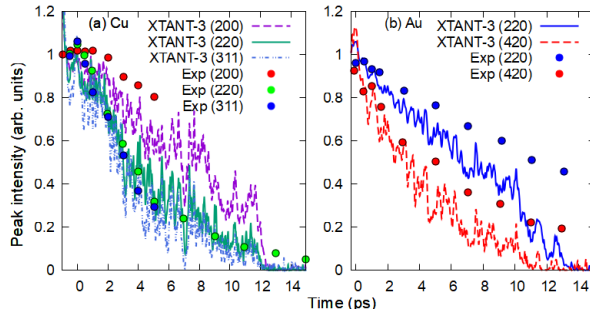


Figure 1. Diffraction peak intensities after ultrafast irradiation. (a) Copper irradiated with $\lambda=400$ nm wavelength pulse, $\tau=130$ fs FWHM duration, $D=0.83$ eV/atom absorbed dose; (b) Gold irradiated with $\lambda=400$ nm, $\tau=130$ fs, $D=0.69$ eV/atom. Lines are simulated with XTANT-3, and circles are experimental data for copper [26] and gold [27].

Nevertheless, up to the time of ~ 10 ps, the model describes the experimental data with an acceptable precision to draw meaningful conclusions. We perform two types of analysis below: (i) under the assumption of the constant Debye temperature, θ_D , we extract the evolution of the atomic temperature from the Debye-Waller factor from Eq.(2) (labeled below as T_{DW} , replacing T_a). (ii) We use the actual atomic kinetic temperature in the simulation ($T_a=2/3E_{kin}$, average

kinetic energy of atoms in the simulation box) to extract the evolution of the Debye temperature from Eq.(2).

Figure 2 displays the comparison of the actual atomic temperature ($T_a=2/3E_{kin}$) in the simulation, and the temperature extracted from the Debye-Waller analysis of the diffraction peak intensities from Figure 1 (T_{DW} , both, calculated and experimental). This comparison shows that the estimated T_{DW} agrees very well with the experimental temperature from the DW factor, further validating the simulation. Both, however, are different from the actual atomic temperature in the simulation of copper and gold, revealing the problem with the extraction of the atomic temperature from the diffraction peak intensities *via* the DW analysis.

We thus conclude that the DW analysis produces erroneous estimates of the atomic temperature if the evolution of the Debye temperature is not included in the analysis. It is associated with the fact that not all the atomic motion is related to the fluctuations around the equilibrium atomic positions – there is a change in the equilibrium positions themselves due to nonthermal effects (phonon hardening).

This failure of the Debye-Waller analysis is even more obvious in the case of nonthermal phase transition in silicon and diamond (Figure 2 c and d). Under drastic changes of the interatomic potential, the DW factor predicts atomic temperature orders of magnitude different from the actual atomic temperature in the same self-consistent simulation.

A further comparison with other definitions of the transient (nonequilibrium) atomic temperatures (the configurational atomic temperature, T_{conf} , associated with the potential energy of atoms [36]), demonstrates that the influence of the atomic nonequilibrium here is minor. The extracted T_{DW} differs drastically from both definitions of the atomic temperature, thus, not being associated with the nonequilibrium atomic state, but revealing a failure of the DW analysis itself.

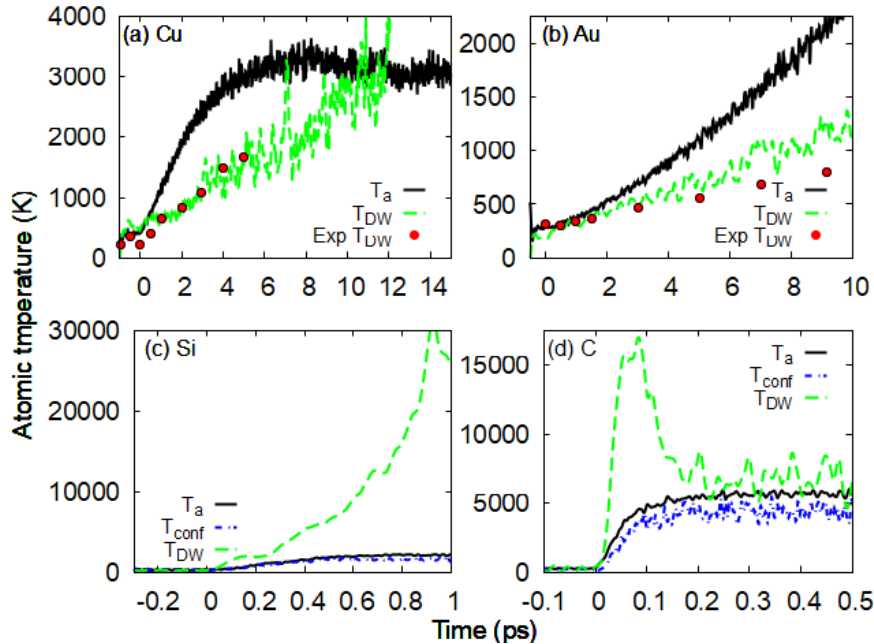


Figure 2. Evolution of the atomic temperature after ultrafast irradiation. (a) Copper irradiated with $\lambda=400$ nm wavelength pulse, $\tau=130$ fs FWHM duration, $D=0.83$ eV/atom absorbed dose; (b) Gold irradiated with $\lambda=400$ nm, $\tau=130$ fs, $D=0.69$

eV/atom; (c) Silicon irradiated with $\hbar\omega=92$ eV photon energy, $\tau=10$ fs, $D=1.1$ eV/atom; (d) Diamond irradiated with $\hbar\omega=92$ eV, $\tau=10$ fs, $D=1.5$ eV/atom. Solid black lines are calculated atomic temperature in the simulation, T_a ; dashed green lines are atomic temperature extracted from the simulated diffraction peaks via Debye-Waller analysis, T_{DW} , assuming constant Debye temperature (345 K in Cu, 170 K in Au, 770 K in Si, and 2500 K in C); red circles are Debye-Waller atomic temperature extracted from experimentally-measured diffraction peaks for copper [26] and gold [27]; blue dash-dotted lines in Si and C are calculated configurational temperatures, T_{conf} .

Now, using the transient kinetic atomic temperature in the simulation and the diffraction peaks evolution (Figure 1), we performe the second type of analysis and extracted the Debye temperature from Eqs. (1,2) for the four studied materials, see Figure 3. First, we notice that this procedure of the dynamical calculation of the Debye temperature produces adequate values for the materials before irradiation (negative times in Figure 3): ~ 300 K in Cu (vs. experimental value of 320 K); ~ 175 K in Au (exp. 170 K); ~ 850 K in Si (exp. 770 K); and ~ 2500 K in diamond (exp. ~ 2000 K), thereby validating this method of evaluation of θ_D in a simulation. We also note that the extraction of the θ_D does not need a specific choice of diffraction peaks, indicating the robustness of the approach. This leads us to a hypothesis that the Debye temperature remains a meaningful and measurable material property even in a nonequilibrium state of matter.

Then, we see that the Debye temperature changes noticeably after the electronic excitation of materials: in Cu, it rises from 320 K to over 500 K by the time of 2 ps and slowly reduces afterward. After the onset of melting, different peaks produce different values of θ_D , which we interpret as the notion that the Debye temperature (maximal phonon frequency) loses its meaning upon the loss of structure in the material.

In irradiated gold, the Debye temperature rises to ~ 250 K due to atomic heating, after the initial small drop to ~ 150 K due to purely electronic excitation (as was discussed in [27,28]). In silicon and diamond, the changes in θ_D are significant, in accord with the ultrafast nonthermal phase transitions [31].

Since the DW factor is $\sim \theta_D^2$, the extraction of the atomic temperature is very sensitive to the changes in the Debye temperature.

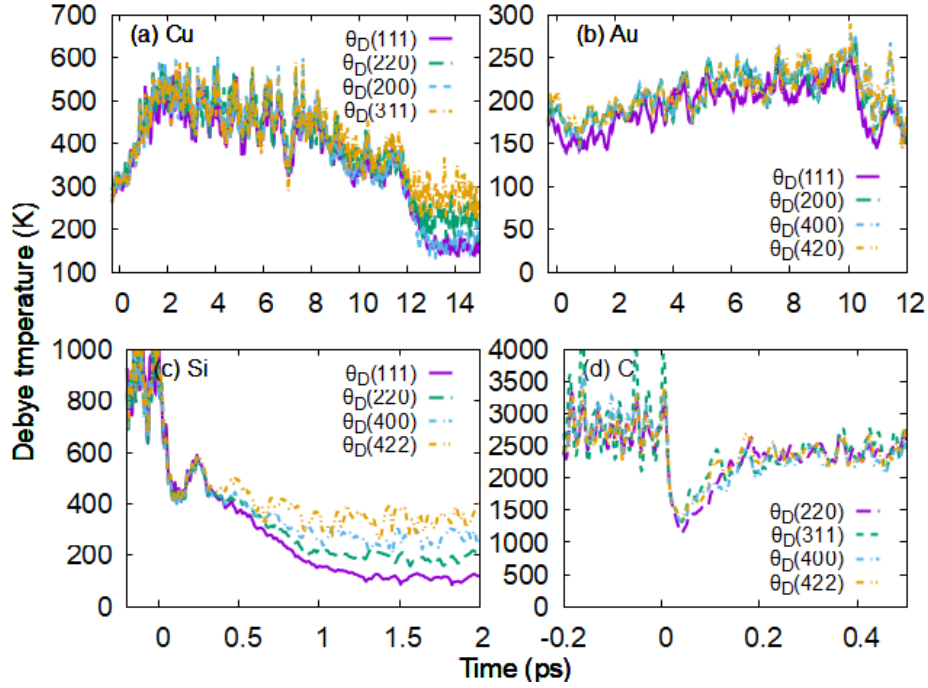


Figure 3. Evolution of the Debye temperature after ultrafast irradiation, extracted from the various diffraction peaks (denoted in the legends), simulated with XTANT-3. (a) Copper irradiated with $\lambda=400$ nm wavelength pulse, $\tau=130$ fs FWHM duration, $D=0.83$ eV/atom absorbed dose; (b) Gold irradiated with $\lambda=400$ nm, $\tau=130$ fs, $D=0.69$ eV/atom; (c) Silicon irradiated with $\hbar\omega=92$ eV photon energy, $\tau=10$ fs, $D=1.1$ eV/atom; (d) Diamond irradiated with $\hbar\omega=92$ eV, $\tau=10$ fs, $D=1.5$ eV/atom.

Conclusions

We thus conclude that the evolution of the Debye temperature must necessarily be considered when extracting the transient atomic temperature from the Debye-Waller analysis. Assuming the Debye temperature constant may produce large deviations from the actual atomic temperature, due to the sensitivity of the DW factor to the Debye temperature. The problem is especially important for materials where the nonthermal effects are present (covalent and ionic materials), but even in metals, the difference may be noticeable. Erroneous estimates of the atomic temperature may lead to incorrect estimates of the electron-phonon coupling parameter and other related quantities.

Acknowledgements

Computational resources were provided by the e-INFRA CZ project (ID:90254), supported by the Ministry of Education, Youth and Sports of the Czech Republic. The author thanks the financial support from the Czech Ministry of Education, Youth, and Sports (grant nr. LM2023068), and from the European Commission Horizon MSCA-SE Project MAMBA [HORIZON-MSCA-SE-2022 GAN 101131245].

References

- [1] F. Graziani, M. P. Desjarlais, R. Redmer, and S. B. Trickey (Eds), *Frontiers and Challenges in Warm Dense Matter* (Springer-Verlag, New York, 2014).
- [2] S. K. Sundaram and E. Mazur, *Inducing and Probing Non-Thermal Transitions in*

- Semiconductors Using Femtosecond Laser Pulses.*, Nat. Mater. **1**, 217 (2002).
- [3] C. W. Siders, A. Cavalleri, K. Sokolowski-Tinten, C. Tóth, T. Guo, M. Kammler, M. H. von Hoegen, K. R. Wilson, D. von der Linde, and C. P. J. Barty, *Detection of Nonthermal Melting by Ultrafast X-Ray Diffraction*, Science **286**, 1340 (1999).
- [4] N. Medvedev, R. Voronkov, and A. E. Volkov, *Metallic Water: Transient State under Ultrafast Electronic Excitation*, J. Chem. Phys. **158**, 074501 (2023).
- [5] M. Lang, F. Zhang, J. Zhang, J. Wang, B. Schuster, C. Trautmann, R. Neumann, U. Becker, and R. C. Ewing, *Nanoscale Manipulation of the Properties of Solids at High Pressure with Relativistic Heavy Ions*, Nat. Mater. **8**, 793 (2009).
- [6] A. P. Solomon, E. C. O’Quinn, J. Liu, I. M. Gussev, X. Guo, J. Neuefeind, C. Trautmann, R. C. Ewing, G. Baldinozzi, and M. K. Lang, *Atomic-Scale Structure of ZrO₂: Formation of Metastable Polymorphs*, Sci. Adv. **11**, 5943 (2025).
- [7] L. Rapp, B. Haberl, C. J. Pickard, J. E. Bradby, E. G. Gamaly, J. S. Williams, and A. V. Rode, *Experimental Evidence of New Tetragonal Polymorphs of Silicon Formed through Ultrafast Laser-Induced Confined Microexplosion*, Nat. Commun. **2015** 61 **6**, 7555 (2015).
- [8] A. Ng, *Outstanding Questions in Electron-Ion Energy Relaxation, Lattice Stability, and Dielectric Function of Warm Dense Matter*, Int. J. Quantum Chem. **112**, 150 (2012).
- [9] A. Ng, *Progress in the Study of Electron–Ion Coupling in Nonequilibrium Warm Dense Au and Cu*, Phys. Rep. **1089**, 1 (2024).
- [10] M. V Shugaev et al., *Fundamentals of Ultrafast Laser-Material Interaction*, MRS Bull. **41**, 960 (2016).
- [11] B. Rethfeld, D. S. Ivanov, M. E. Garcia, and S. I. Anisimov, *Modelling Ultrafast Laser Ablation*, J. Phys. D: Appl. Phys. **50**, 193001 (2017).
- [12] B. Rethfeld, A. Kaiser, M. Vicanek, and G. Simon, *Ultrafast Dynamics of Nonequilibrium Electrons in Metals under Femtosecond Laser Irradiation*, Phys. Rev. B **65**, 214303 (2002).
- [13] N. S. Shcheblanov and T. E. Itina, *Femtosecond Laser Interactions with Dielectric Materials: Insights of a Detailed Modeling of Electronic Excitation and Relaxation Processes*, Appl. Phys. A **110**, 579 (2012).
- [14] N. Medvedev, *Electronic Nonequilibrium Effect in Ultrafast-Laser-Irradiated Solids*, Phys. Scr. **99**, 015934 (2024).
- [15] A. Kaiser, B. Rethfeld, M. Vicanek, and G. Simon, *Microscopic Processes in Dielectrics under Irradiation by Subpicosecond Laser Pulses*, Phys. Rev. B **61**, 11437 (2000).
- [16] I. M. Lifshits, M. I. Kaganov, and L. V. Tanatarov, *On the Theory of Radiation-Induced Changes in Metals*, J. Nucl. Energy. Part A. React. Sci. **12**, 69 (1960).
- [17] L. Waldecker, R. Bertoni, R. Ernstorfer, and J. Vorberger, *Electron-Phonon Coupling and Energy Flow in a Simple Metal beyond the Two-Temperature Approximation*, Phys. Rev. X **6**, 021003 (2016).
- [18] J. Xu, X. Huang, Y. Sheng, Q. Sun, H. Zhang, H. Bao, and Y. Yue, *Direct Observation of Substantial Phonon Nonequilibrium Near Nanoscale Hotspots in Gallium Nitride*,

- Adv. Sci. **12**, 2411040 (2025).
- [19] A. Descamps et al., *Evidence for Phonon Hardening in Laser-Excited Gold Using x-Ray Diffraction at a Hard x-Ray Free Electron Laser*, Sci. Adv. **10**, 5272 (2024).
- [20] V. Recoules and J.-P. Crocombette, *Ab Initio Determination of Electrical and Thermal Conductivity of Liquid Aluminum*, Phys. Rev. B **72**, 104202 (2005).
- [21] A. Rudenko and D. Rolles, *Time-Resolved Studies with FELs*, J. Electron Spectros. Relat. Phenomena **204**, 228 (2015).
- [22] A. Marinelli et al., *High-Intensity Double-Pulse X-Ray Free-Electron Laser*, Nat. Commun. **6**, 6369 (2015).
- [23] G. Kang et al., *Nonequilibrium Electron-Phonon and Electron-Ion Couplings in Warm Dense Copper*, Appl. Surf. Sci. **713**, 164304 (2025).
- [24] B. I. Cho et al., *Electronic Structure of Warm Dense Copper Studied by Ultrafast X-Ray Absorption Spectroscopy*, Phys. Rev. Lett. **106**, 167601 (2011).
- [25] L. Lecherbourg, V. Recoules, P. Renaudin, and F. Dorchie, *Dynamics of Femtosecond Heated Warm Dense Copper with Time-Resolved L3-Edge XANES*, Philos. Trans. R. Soc. A Math. Phys. Eng. Sci. **381**, 20220214 (2023).
- [26] M. Z. Mo et al., *Probing the Atomic Dynamics of Ultrafast Melting with Femtosecond Electron Diffraction*, (2025)
[arXiv:2511.05054](https://arxiv.org/abs/2511.05054) [cond-mat.mtrl-sci].
- [27] M. Z. Mo et al., *Heterogeneous to Homogeneous Melting Transition Visualized with Ultrafast Electron Diffraction*, Science **360**, 1451 (2018).
- [28] R. Ernstorfer, M. Harb, C. T. Hebeisen, G. Sciaini, T. Dartigalongue, and R. J. D. Miller, *The Formation of Warm Dense Matter: Experimental Evidence for Electronic Bond Hardening in Gold*, Science **323**, 1033 (2009).
- [29] M. Z. Mo et al., *Determination of the Electron-Lattice Coupling Strength of Copper with Ultrafast MeV Electron Diffraction*, Rev. Sci. Instrum. **89**, 10 (2018).
- [30] N. Medvedev, *XTANT-3 [Computer Software]*,
<https://zenodo.org/badge/latestdoi/490215542>
- [31] N. Medvedev, V. Tkachenko, V. Lipp, Z. Li, and B. Ziaja, *Various Damage Mechanisms in Carbon and Silicon Materials under Femtosecond X-Ray Irradiation*, 4open **1**, 3 (2018).
- [32] N. Medvedev and I. Milov, *Electron-Phonon Coupling in Metals at High Electronic Temperatures*, Phys. Rev. B **102**, 064302 (2020).
- [33] N. Medvedev and I. Milov, *Nonthermal Phase Transitions in Metals*, Sci. Rep. **10**, 12775 (2020).
- [34] J. M. . Cowley, *Diffraction Physics*, 3rd ed. (Elsevier Science B.V., 1995).
- [35] *EPICS2025*, <https://nuclear.llnl.gov/EPICS/index.html>.
- [36] N. Medvedev and A. E. Volkov, *Multitemperature Atomic Ensemble: Nonequilibrium Evolution after Ultrafast Electronic Excitation*, Phys. Rev. E **110**, 024142 (2024)."

Supplementary Materials

for

“Limitations of Debye-Waller lattice temperature extraction under electronic excitation”

N. Medvedev^{1,2,†}, M. Kopecky¹, J. Chalupsky¹ L. Juha^{1,2}

1) Institute of Physics, Czech Academy of Sciences, Na Slovance 1999/2, 182 00 Prague 8, Czechia

2) Institute of Plasma Physics, Czech Academy of Sciences, Za Slovankou 3, 182 00 Prague 8, Czechia

Numerical Parameters

The models combined in XTANT-3 are described in detail in its manual [1]. Here, we list numerical parameters used in the current simulation of the selected materials for reproducibility of the results.

The photoabsorption cross sections, atomic ionization potentials, Auger decay times, and atomic form factors used are from the EPICS2025 database [2]. For electron impact ionization, the complex-dielectric function formalism with the single-pole approximation is used [3]. For low-electron electron-electron scattering, the instantaneous relaxation-time approximation is applied, relaxing electrons to the Fermi-Dirac distribution [4]. The nonperturbative dynamical coupling approach describes the electron-phonon (electron-ion) coupling between the electrons and atoms [5].

The following transferable tight-binding parametrizations are applied: for Cu, matsci-0-3 (with the basis set sp^3d^5) [6]; for Au, auorg-1-1 (basis set sp^3d^5) [7]; for Si, from Kwon *et al.* (basis set sp^3) [8]; and for C, from Xu *et al.* (basis set sp^3) [9].

The simulation boxes contained 256 atoms for Cu and Au (4x4x4 unit cells in the face-centered cubic (fcc) structure), and 512 atoms for Si and C (4x4x4 unit cells in the diamond structure). Martyna-Tuckerman 4th order algorithm for propagation of atomic trajectories in the molecular dynamics (MD) simulation is used with the timestep of 0.5 fs for Cu, Au, and Si, and 0.2 fs for diamond [10]. In all reported simulations, the NVE (microcanonical) ensemble is applied with periodic boundary conditions for the supercell.

The following irradiation parameters are simulated: for copper, the pulse of $\lambda=400$ nm wavelength, $\tau=130$ fs full-width at half-maximum (FWHM) duration, $D=0.83$ eV/atom absorbed dose; for gold, $\lambda=400$ nm, $\tau=130$ fs, $D=0.69$ eV/atom; for Si, the photon energy of $\hbar\omega=92$ eV was used, $\tau=10$ fs, $D=1.1$ eV/atom (above the threshold of nonthermal melting in the nonadiabatic simulation [11]); and for diamond, $\hbar\omega=92$ eV, $\tau=10$ fs, $D=1.5$ eV/atom (above the nonthermal graphitization threshold in the nonadiabatic simulation [12]).

Medium fluences from the corresponding experiments' peaks for copper [12] and gold [13] are used because the highest reported fluences are approaching (or beyond) the limits of applicability of the XTANT-3 simulation tool. The melting takes place in the simulation

[†] Corresponding author: nikita.medvedev@fzu.cz; ORCID: 0000-0003-0491-1090

significantly faster than in the experiment, due to finite-size effects and limitations of the tight-binding parametrizations independent of the electronic temperature, which limits quantitative comparisons to not-too-high excitations. In the opposite case, simulation of the lowest reported doses suffers from the consumption of computational resources: low doses require prohibitively long times for a noticeable rise in the atomic temperature and equilibration with the electronic one. Thus, the current simulations are limited to the medium fluences (absorbed doses). Nevertheless, it is sufficient to illustrate the discussed effects and reveal the importance of the Debye temperature evolution for the extraction of the atomic temperature from the Debye-Waller analysis of the diffraction peak intensities.

Inensitivity of the T_{DW} to the choice of the diffraction peak

Figure 4 illustrates that the atomic temperature extracted from any diffraction peak is identical, and different from the actual atomic temperature in the simulation. The insensitivity of the analysis to the choice of the diffraction peak supports the robustness of the proposed simulation method and conclusions drawn.

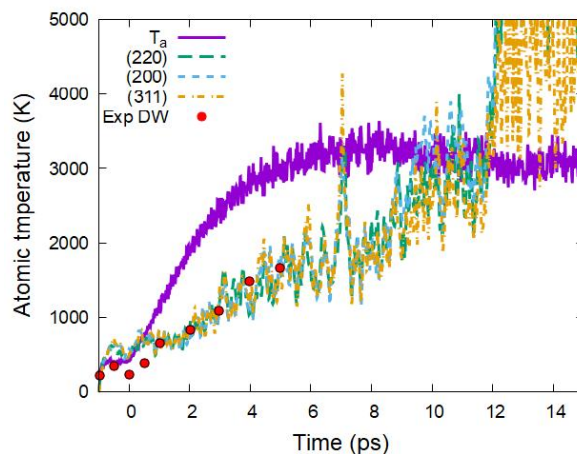


Figure 4. Evolution of the atomic temperature in time after ultrafast irradiation of copper with a 400 nm wavelength pulse, 130 fs FWHM duration, 0.83 eV/atom absorbed dose. Solid line is calculated atomic temperature, T_a ; dashed lines are atomic temperature extracted from the simulated diffraction peaks via Debye-Waller analysis of various diffraction peaks, T_{DW} , assuming constant Debye temperature. Red circles are the Debye-Waller atomic temperature extracted from experimentally measured diffraction peaks [13].

Electron temperature

The evaluated electronic temperature evolution and equilibration with the atomic one in the four irradiation scenarios are shown in Figure 5. Different timescales of equilibration reflect the different electron-phonon coupling in the studied materials (see below), as well as the presence and strength of the nonthermal effects.

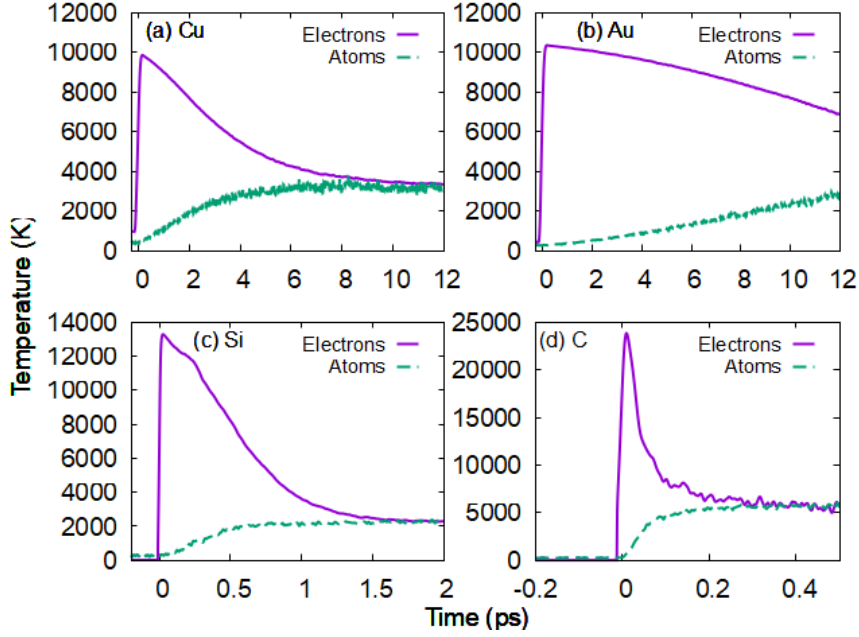


Figure 5. Evolution of the electronic and atomic temperatures after ultrafast irradiation. (a) Copper irradiated with 400 nm wavelength pulse, 130 fs FWHM duration, 0.83 eV/atom absorbed dose; (b) Gold irradiated with 400 nm wavelength pulse, 130 fs FWHM duration, 0.69 eV/atom absorbed dose; (c) Silicon irradiated with 92 eV photon energy pulse, 10 fs FWHM duration, 1.1 eV/atom absorbed dose; (d) Diamond irradiated with 92 eV photon energy pulse, 10 fs FWHM duration, 1.5 eV/atom absorbed dose.

Electron-phonon coupling

The time-resolved electron-phonon coupling parameter in the four materials is shown in Figure 6. As discussed previously [5,14], the coupling parameter depends on both the electronic temperature (more generally, electron distribution function) and the atomic temperature. Strong oscillations observed by the end of the simulation reflect the fact that the coupling parameter is undefined for equal electronic and atomic temperature (see their equilibration in Figure 5).

Note that the coupling parameter in gold is different from the one extracted by means of fitting the two-temperature model to the Debye-Waller temperature [15]. This is a consequence of the neglect of the evolution of the Debye temperature in the experimental DW analysis.

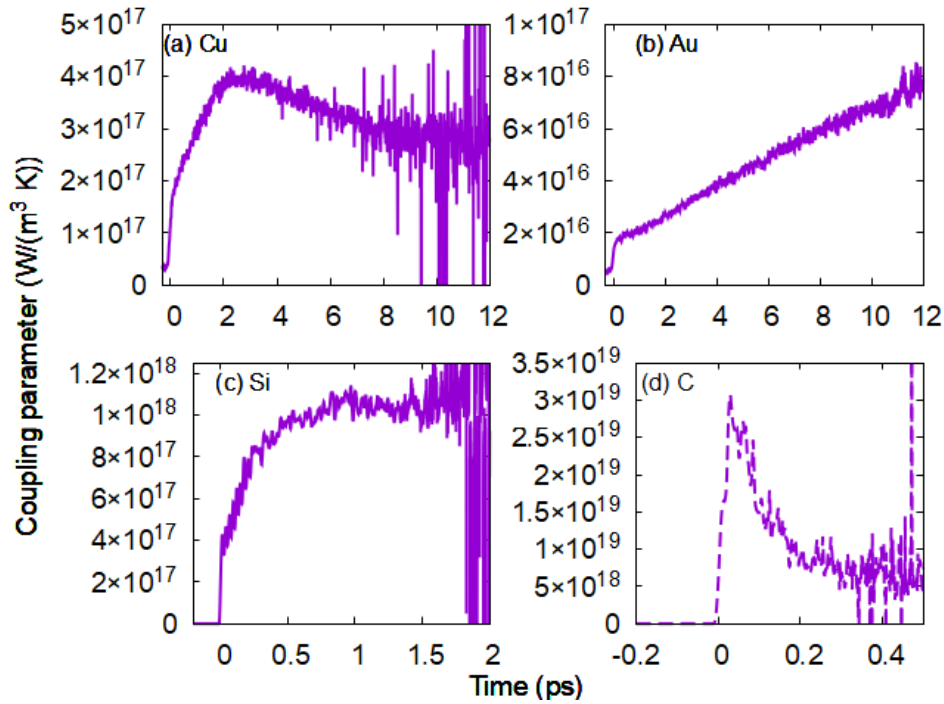


Figure 6. Evolution of the electron-phonon coupling parameter in time after ultrafast irradiation. (a) Copper irradiated with 400 nm wavelength pulse, 130 fs FWHM duration, 0.83 eV/atom absorbed dose; (b) Gold irradiated with 400 nm wavelength pulse, 130 fs FWHM duration, 0.69 eV/atom absorbed dose; (c) Silicon irradiated with 92 eV photon energy pulse, 10 fs FWHM duration, 1.1 eV/atom absorbed dose; (d) Diamond irradiated with 92 eV photon energy pulse, 10 fs FWHM duration, 1.5 eV/atom absorbed dose.

References

- [1] N. Medvedev, *XTANT-3* [Computer Software], <https://zenodo.org/badge/latest/doi/490215542>
- [2] *EPICS2025*, <https://nuclear.llnl.gov/EPICS/index.html>.
- [3] N. Medvedev, F. Akhmetov, R. A. Rymzhanov, R. Voronkov, and A. E. Volkov, *Modeling Time-Resolved Kinetics in Solids Induced by Extreme Electronic Excitation*, *Adv. Theory Simulations* **5**, 2200091 (2022).
- [4] N. Medvedev, *Electronic Nonequilibrium Effect in Ultrafast-Laser-Irradiated Solids*, *Phys. Scr.* **99**, 015934 (2024).
- [5] N. Medvedev and I. Milov, *Electron-Phonon Coupling in Metals at High Electronic Temperatures*, *Phys. Rev. B* **102**, 064302 (2020).
- [6] J. Frenzel, A. F. Oliveira, N. Jardillier, T. Heine, and G. Seifert, *Semi-Relativistic, Self-Consistent Charge Slater-Koster Tables for Density-Functional Based Tight-Binding (DFTB) for Materials Science Simulations.*, 2009.
- [7] A. Fihey, C. Hettich, J. Touzeau, F. Maurel, A. Perrier, C. Köhler, B. Aradi, and T. Frauenheim, *SCC-DFTB Parameters for Simulating Hybrid Gold-Thiolates Compounds*, *J. Comput. Chem.* **36**, 2075 (2015).
- [8] I. Kwon, R. Biswas, C. Wang, K. Ho, and C. Soukoulis, *Transferable Tight-Binding*

- Models for Silicon*, Phys. Rev. B **49**, 7242 (1994).
- [9] C. H. Xu, C. Z. Wang, C. T. Chan, and K. M. Ho, *A Transferable Tight-Binding Potential for Carbon*, J. Phys. Condens. Matter **4**, 6047 (1992).
- [10] G. J. Martyna and M. E. Tuckerman, *Symplectic Reversible Integrators: Predictor–Corrector Methods*, J. Chem. Phys. **102**, 8071 (1995).
- [11] N. Medvedev, Z. Li, V. Tkachenko, and B. Ziaja, *Electron-Ion Coupling in Semiconductors beyond Fermi’s Golden Rule*, Phys. Rev. B **95**, 014309 (2017).
- [12] N. Medvedev, Z. Kuglerová, M. Makita, J. Chalupský, and L. Juha, *Damage Threshold in Pre-Heated Optical Materials Exposed to Intense X-Rays*, Opt. Mater. Express **13**, 808 (2023).
- [13] M. Z. Mo et al., *Probing the Atomic Dynamics of Ultrafast Melting with Femtosecond Electron Diffraction*, (2025).
- [14] N. Medvedev, *Electron-Phonon Coupling in Semiconductors at High Electronic Temperatures*, Phys. Rev. B **108**, 144305 (2023).
- [15] M.Z. Mo et al., *Heterogeneous to Homogeneous Melting Transition Visualized with Ultrafast Electron Diffraction*, Science **360**, 1451 (2018).